ACS APPLIED MATERIALS & INTERFACES

Research Article

www.acsami.org

Interfacial Engineering Importance of Bilayered ZnO Cathode Buffer on the Photovoltaic Performance of Inverted Organic Solar Cells

Rohan B. Ambade,[†] Swapnil B. Ambade,[†] Rajaram S. Mane,[‡] and Soo-Hyoung Lee*[,†]

[†]School of Semiconductor and Chemical Engineering, Chonbuk National University, 664-14, 1-ga Deokjin-dong, Deokjin-gu, Jeonju, Jeonbuk 561-756, Republic of Korea

[‡]Center for Nanomaterials and Energy Devices, Swami Ramanand Teerth Marathwada University, Dnyanteerth, Vishnupuri, Nanded, 431606, India

Supporting Information

ABSTRACT: The role of cathode buffer layer (CBL) is crucial in determining the power conversion efficiency (PCE) of inverted organic solar cells (IOSCs). The hallmarks of a promising CBL include high transparency, ideal energy levels, and tendency to offer good interfacial contact with the organic bulk-heterojunction (BHJ) layers. Zinc oxide (ZnO), with its ability to form numerous morphologies in juxtaposition to its excellent electron affinity, solution processability, and good transparency is an ideal CBL material for IOSCs. Technically, when CBL is sandwiched between the BHJ active layer and the indium−tin-oxide (ITO) cathode, it performs two functions, namely, electron collection from the photoactive layer that is effectively carried out by morphologies like nanoparticles or nanoridges obtained by ZnO sol−gel (ZnO SG) method through an accumulation of individual nanoparticles and, second, transport of collected electrons toward the cathode, which is more effectively manifested by one-dimensional (1D) nanostructures like ZnO nanorods (ZnO NRs). This work presents the use of bilayered ZnO CBL in IOSCs of poly(3-hexylthiophene) (P3HT)/[6, 6]-phenyl-C_{60}-butyric acid methyl ester (PCBM) to overcome the limitations offered by a conventionally used single layer CBL. We found that the PCE of IOSCs with an appropriate bilayer CBL comprising of ZnO NRs/ZnO SG is ∼18.21% higher than those containing ZnO SG/ZnO NRs. We believe that, in bilayer ZnO NRs/ZnO SG, ZnO SG collects electrons effectively from photoactive layer while ZnO NRs transport them further to ITO resulting significant increase in the photocurrent to achieve highest PCE of 3.70%. The enhancement in performance was obtained through improved interfacial engineering, enhanced electrical properties, and reduced surface/bulk defects in bilayer ZnO NRs/ZnO SG. This study demonstrates that the novel bilayer ZnO CBL approach of electron collection/transport would overcome crucial interfacial recombination issues and contribute in enhancing PCE of IOSCs.

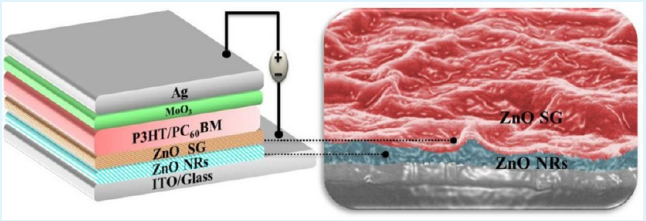

KEYWORDS: *inverted organic solar cells, cathode buffer layer, ZnO sol−gel/nanorods, bilayer, morphology, interfacial engineering*

INTRODUCTION

Organic solar cells (OSCs) have attracted immense interest globally owing to their ease of fabrication, low-temperature solution processability, mechanical flexibility using plastic substrates, light weight, and importantly low cost.[1−5] Bulk heterojunction (BHJ) solar cells that comprise a photoactive blend of electron donor/acceptor (P3HT:PCBM) by forming a bicontinuous network between cathode and anode have recently received great attention due to their relatively low production cost and high PCE up to 10%.[6−10] The structure of conventional OSCs typically consists of a transparent conductive anode (e.g., ITO), an anode buffer layer of acidic poly(3,4-ethyl-enedioxythiophene)/poly(styrenesulfonate) (PEDOT: PSS), a low work function metal cathode (e.g., Al, Ca), and a blended BHJ conjugated polymer/fullerene derivative photoactive layer sandwiched between these two electrodes. However, the strong acidic, corrosive and hygroscopic nature of the PEDOT:PSS layer is unfavorable to ITO, and the low work function of the metallic cathode that is susceptible to oxidation upon exposure to oxygen and water vapor leads to the degradation and poor stability of OSCs.[11] Moreover, it has been demonstrated recently that vertical phase separation spontaneously occurs in polymer active layer with the fullerene derivative rich adjacent to the substrate interface.[12] To overcome these challenges in the regular device structure, inverted organic solar cells (IOSCs) have been developed as a promising alternative for obtaining high device performance, in which ITO is used as the bottom cathode to collect electrons instead of the top metal electrode and high work function metal (Ag, Au, etc.) as anode to collect holes.[13−15] The real key to success for enhancement in PCE of OSCs is the use of inorganic materials (metal oxides) as CBLs.[16,17] As a primary requirement, a CBL should be stable, have good transparency in the visible spectral region, should collect and effectively

Received: December 27, 2014
Accepted: March 24, 2015
Published: March 24, 2015

DOI: 10.1021/am509125c
ACS Appl. Mater. Interfaces 2015, 7, 7951−7960

transport negatively charged carriers (electrons), should provide an ohmic contact with the acceptor, and offer minimum series resistance.[17−20] Numerous metal oxides such as ZnO,[21,22] titanium oxide (TiO_x),[23] cesium carbonate (Cs_2CO_3),[24] and so forth have been explored to improve electron extraction. These metal oxides are coated on ITO to tune its work function either by thermal evaporation or solution process. Solution processed metal oxides are mostly favored for large area fabrication such as roll-to-roll printing.[17] Among various metal-oxides, ZnO in particular has attracted major attention as CBL because of its high electron mobility, high environmental stability, high transmittance and possibility to form various nanostructures by solution processes, making it fully compatible for roll-to-roll fabrication onto flexible substrates.[16,21,22] Various methods such as sol−gel (SG),[22] hydrothermal,[25] nanoimprint lithography,[26] atomic layer deposition,[27] electrodeposition,[28] and so forth have been explored to prepare different nanostructures of ZnO.

Yang et al. proposed an interesting nanoridge morphology of ZnO for efficient CBL that is obtained using the SG method, owing to its high transparency, ease of synthesis, and excellent electron collection capability.[29] As an additional advantage, nanoridges of ZnO SG are beneficial in improving the interfacial contacts, necessary for charge separation at the interfaces of the photoactive BHJ layers, which simply makes ZnO SG as a promising electron extracting layer. Despite good electron selectivity, the charge transportation in ZnO SG is limited.[30] This is attributed to the complexity in developing a compact layer in between the ITO and the photoactive layer as nanoridges of ZnO SG are typically formed by piling up of gel particles that are structurally relaxed as a result of gradual solvent evaporation caused by slow heating.[29] Recently, we reported that high electron transportation is achieved by using transparent one-dimensional (1D) planar ZnO NRs since they act as well-defined, robust charge transport paths with high carrier mobilities.[25] This is also in accordance with a study by Takanezawa et al., who observed that high performance in IOSCs can be achieved even with very thick photoactive layers of over 450 nm, leading to the maximum utilization of the incident photons.[31]

Inspired by these concepts based on effective electron extraction offered by ZnO SG and faster electron transport provided by 1D ZnO NRs, we designed a novel strategy of forming a bilayer CBL with two distinct nanostructures which play two roles, namely, electron extraction and efficient transportation. Moreover, the bilayer CBL configuration of ZnO NRs/ZnO SG improves the interfacial contact area between photoactive and CBL, beneficial to suppress the recombinations, ultimately resulting in enhancement in PCE, short circuit current density (J_{sc}), and open circuit voltage (V_{oc}) of the device.

This work presents detailed investigations to demonstrate the outstanding effect of bilayer ZnO nanostructures in IOSCs. Two ZnO bilayers of different morphologies, that is, ZnO SG/ZnO NRs (i.e., ZnO NRs coated over ZnO SG) and ZnO NRs/ZnO SG (i.e., ZnO SG coated over ZnO NRs), are systematically engineered. For reference, IOSCs of single ZnO SG and ZnO NRs CBLs are also compared. It is found that the photovoltaic performances of IOSCs are strongly dependent on the bilayer CBL layering sequence which is attributed to the resulting geometry of nanostructure and the interfacial contact that the upper nanostructure forms with the photoactive layer. A maximum PCE of 3.70% is obtained for the IOSCs comprising a bilayer CBL of ZnO NRs/ZnO SG that is ∼18.21% higher than those comprising an inverse bilayer configuration (i.e., ZnO SG/ZnO NRs). Moreover, the PCE in IOSCs of bilayer CBL (ZnO NRs/ZnO SG) is higher as well by ∼14% for IOSCs comprising a single layer CBL (i.e., ZnO SG or ZnO NRs).

RESULTS AND DISCUSSION

Figure 1 depicts architectures of IOSC devices with different bilayer ZnO CBLs used in this work. To observe the influence

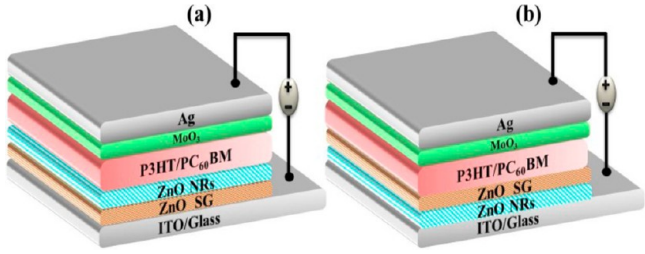

Figure 1. Device architecture of inverted organic solar cells: (a) bilayer ZnO SG/ZnO NRs and (b) bilayer ZnO NRs/ZnO SG.

of bilayer ZnO on the device performance in IOSCs, the surface morphologies of ZnO layers were examined using field-emission scanning electron microscopy (FE-SEM) digital photoimages (Figure 2). The optimized morphologies of all

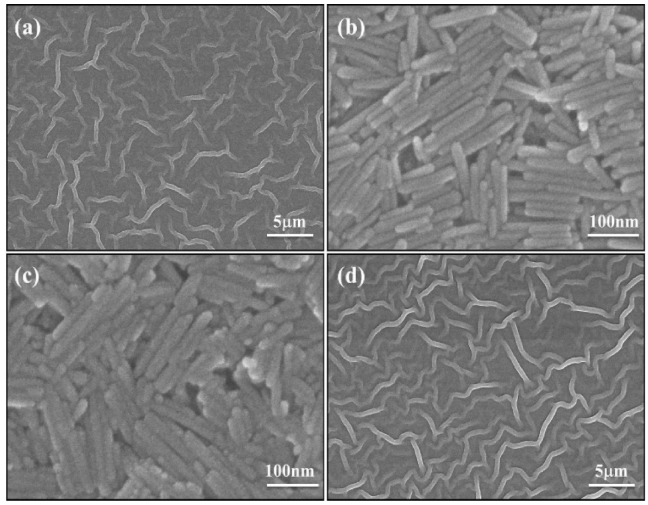

Figure 2. FE-SEM top view images of ZnO CBLs: (a) ZnO SG, (b) ZnO NRs, (c) bilayer ZnO SG/ZnO NRs, and (d) bilayer ZnO NRs/ZnO SG.

the ZnO CBLs used in this work are shown in Figure 2. The morphology of ZnO (Figure 2a) obtained by SG method and annealed at a low temperature of 170 °C for 30 min revealed ∼150 nm thick nanoridges that were separated by a uniform planar surface that was ∼50 nm thick. The distance between two subsequent nanoridges was ∼1 μm. It is interesting to note that the annealing temperature had a major influence on the morphology. With increase in annealing temperature to 270 °C, nanoridges collapse and form nanoparticulate-type morphology (see Figure S1b in the Supporting Information, SI, for more details). Figure 2b presents the morphology of spin- coated 1D planar ZnO NRs that were obtained by a low temperature hydrothermal seedless method according to our previous

DOI: 10.1021/am509125c
ACS Appl. Mater. Interfaces 2015, 7, 7951−7960

report.[25] Spin-coated ZnO NRs are advantageous in controlling the roughness as well as transparency in comparison to vertically grown seeded ZnO NRs. On spin-coating, the whole ITO substrate surface was uniformly covered with dense arrays of ZnO NRs each of ~25 nm diameter and ~100 nm in length. The desired crystallinity of ZnO NRs was obtained by annealing them to 270 °C (Figure 2b) while annealing at 170 °C resulted in amorphous morphology (SI Figure S1d). The morphologies of bilayer ZnO nanostructures used for a sequence of ZnO SG/ZnO NRs and ZnO NRs/ZnO SG are shown in Figure 2c and d. It is clear that the morphology of bilayer CBL is completely distinct from that of single layered ZnO NRs CBL. This is attributed to the difference in the bottom layer on which the ZnO NRs are spin-coated. For the bilayer CBL, the wavy nanoridge structure of ZnO SG in the bottom layer offer a nonuniform surface for the ZnO NRs to coat on them (Figure 2c). Additionally, dual step annealing further distorts the morphology of ZnO NRs. This distortion is attributed to the collapse in nanoridge structure of the bottom layer (ZnO SG) to nanoparticulates as it undergoes dual annealing, once at 170 °C and second when the top layer of ZnO NRs is annealed at 270 °C. To confirm the effect of dual annealing on ZnO SG, ZnO SG was annealed doubly, first at 170 °C, and then at 270 °C which resulted in fine nanoparticles (SI Figure S4a and b). Second, for a much higher annealing condition (270−270 °C), a greater distortion is observed (SI Figure S1i). However, the shape and morphology of ZnO NRs is best maintained for the annealing condition of 170−270 °C (Figure 2c). A high temperature annealing of 270 °C increases the crystallinity of ZnO NRs, which keeps the nanostructure intact over the possibly formed particulates of ZnO SG.

The morphology of second type of bilayer with ZnO NRs/ZnO SG sequence is illustrated in Figure 2d where the presence of homogeneous and comparatively denser nanoridges of ZnO SG compared to single layer of ZnO SG is observed. The width of the nanoridges is reduced to ~0.54 μm (from ~1 μm in single layer ZnO SG). Such dense and homogeneous bilayer ZnO CBL results in improved contact between the CBL and the photoactive layer, which ultimately can lead to enhancement in overall PCE of IOSCs (discussed later).

The crystallinity of bilayer ZnO CBLs was analyzed using X-ray diffraction (XRD; Figure 3). As seen in Figure 3, several sharp peaks relating to hexagonal wurtzite structure are observed. The sharp diffraction peaks, especially the (002) peak shown in Figure 3, for the aligned ZnO NRs/ZnO SG reveal good crystallinity. It is clear that the favorable growth

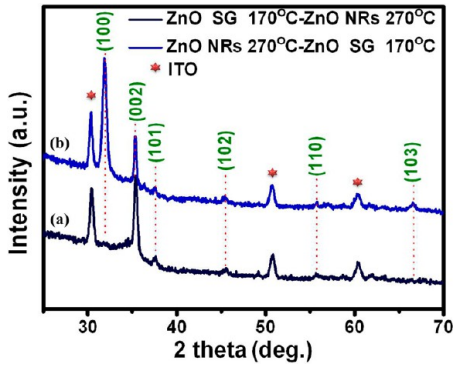

Figure 3. XRD patterns of bilayer ZnO CBLs: (a) ZnO SG/ZnO NRs and (b) ZnO NRs/ZnO SG.

direction of ZnO crystals is (002).[32,33] A minor shift in the (002) diffraction for ZnO NRs/ZnO SG (~0.18°) as compared to ZnO SG/ZnO NRs is indicative of the presence of residual stress and associated strain, which ultimately affects the overall structural properties.[34] For ZnO SG/ZnO NRs, (002) diffraction has a comparatively larger full-width at half-maximum (fwhm) of ~0.29° compared to ZnO NRs/ZnO SG with a lower fwhm value of 0.22° (Figure 3b). This shows that better structural properties can be obtained for ZnO NRs/ZnO SG because of improved mobilities of precursor molecules on the surface resulting from adequate thermal energy. These results are in good agreement with the FE-SEM data as shown in Figure 2c and d. The use of higher boiling point solvents such as 2-methoxyethanol and ethanolamine for ZnO SG, resulted in a strongly preferred orientation of ZnO grain crystals.[35] It is to be noted that the bilayer ZnO NRs/ZnO SG showed sharp (100) peak that arise from perfectly oriented ZnO SG on the uniformly coated ZnO NRs. The absence of (100) peak for ZnO SG/ZnO NRs is attributed to the distortion of SG nanoridges to nanoparticles due to dual annealing of bottom layer ZnO SG that is further coated by ZnO NRs.

Transmittance spectra of bilayer ZnO CBLs formed on a glass substrate (Figure 4) show high transmittance (>95%) in

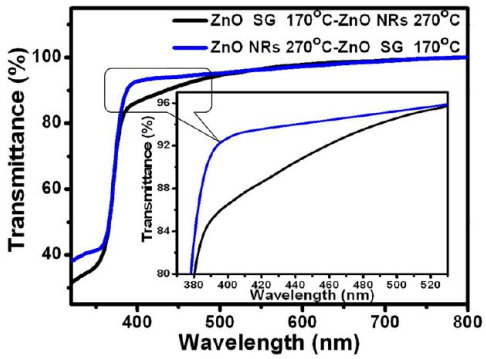

Figure 4. Transmittance spectra of bilayer ZnO CBLs.

the visible spectral range for both the films. From the inset of Figure 4, it is clear that the transmittance of ZnO NRs/ZnO SG is higher as compared to ZnO SG/ZnO NRs. This is probably due to lower optical scattering caused by the densification of grains followed by grain growth and diminution of grain boundary density.[36]

The chemical elemental analysis on both bilayer ZnO CBLs was investigated by X-ray photoelectron spectroscopy (XPS) analysis. The calibration of binding energies was done by taking carbon (C 1s peak at 284.6 eV) as a reference. Figure 5 shows Zn $2p_{3/2}$, Zn $2p_{1/2}$, and O 1s core level XPS spectra of both the bilayer ZnO CBLs with different morphologies. The difference between Zn $2p_{3/2}$ and Zn $2p_{1/2}$ binding energies of ZnO bilayer CBLs is ~23.02 eV, which is in good agreement with the standard value of ~22.97 eV for Zn^{2+}.[37] Figure 5a shows that the Zn $2p_{3/2}$ peak for bilayer ZnO NRs/ZnO SG shifts toward lower binding energy by 0.05 eV due to its dense morphology signifying that more Zn atoms are compelled to O atoms as compared to that in ZnO SG/ZnO NRs that typically has a distorted morphology.

The O 1s XPS spectra as shown in Figure 5c and d demonstrate asymmetric shapes indicating that oxygen species are present in the nearby areas. Deconvolution of peaks was

DOI: 10.1021/am509125c
ACS Appl. Mater. Interfaces 2015, 7, 7951−7960

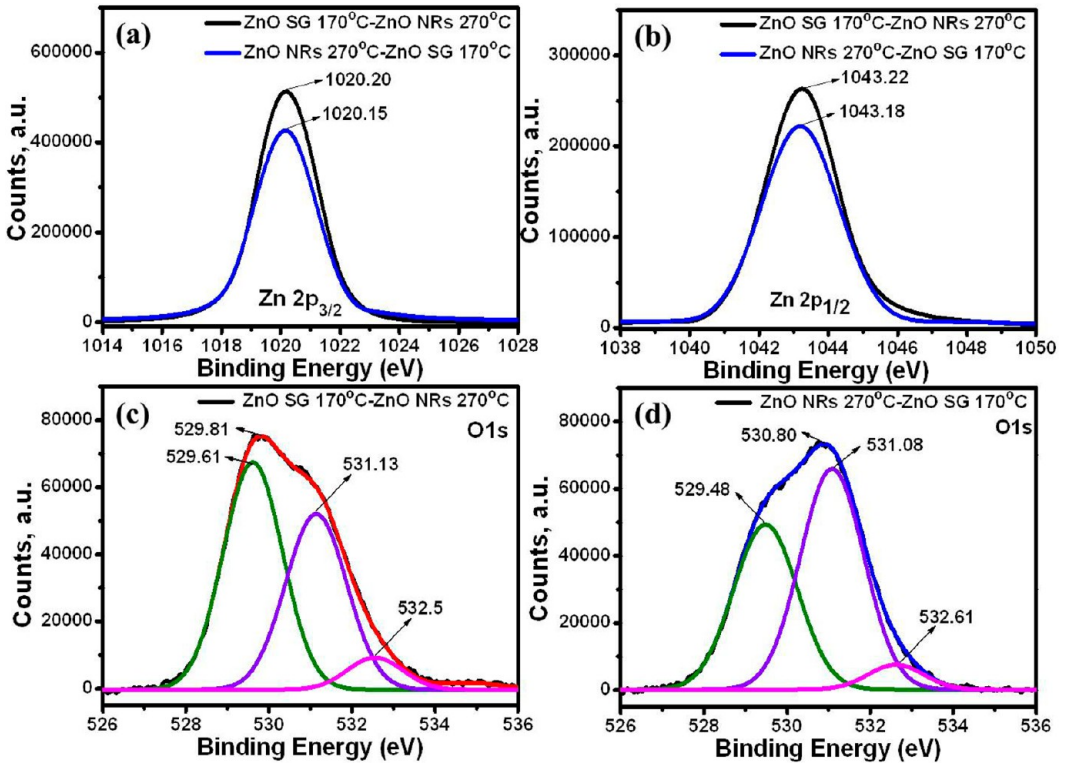

Figure 5. XPS spectra of bilayer ZnO CBLs: (a) Zn $2p_{3/2}$, (b) Zn $2p_{1/2}$, and (c, d) O 1s.

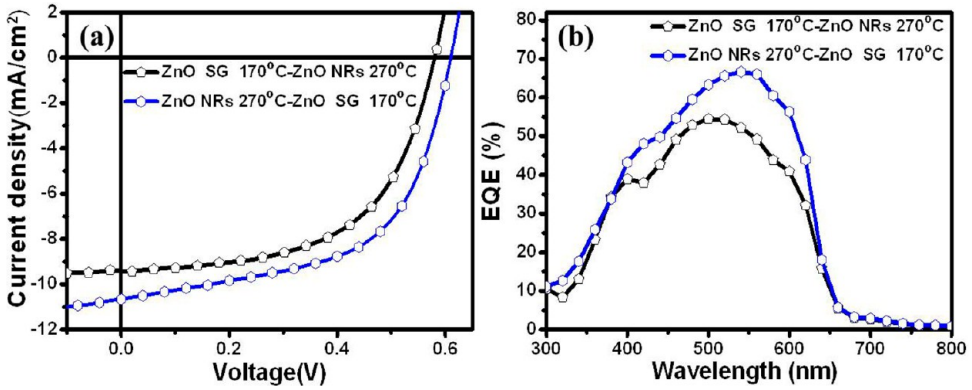

Figure 6. Photovoltaic performance, that is, (a) *J*−*V* and (b) EQE measurements of bilayer ZnO CBLs at optimized annealing temperatures in IOSC.

Table 1. PCE Performance Parameters of the Devices Based on P3HT:$PC_{60}BM$ Blends with Bilayer ZnO SG/ZnO NRs and ZnO NRs/ZnO SG CBLs as Electron Transporting/Collecting Layers at Different Annealing Temperatures

bilayer ZnO CBL	J_{sc} (mA/cm^2)	V_{oc} (V)	FF (%)	PCE (%) best (avg)
ZnO SG 170 °C/ZnO NRs 270 °C	9.48 (9.45)	0.58 (0.58)	57 (57)	3.13 (3.11)
ZnO NRs 270 °C/ZnO SG 170 °C	10.66 (10.58)	0.61 (0.609)	57 (57)	3.70 (3.68)

*PCE data averaged for 40 devices.

carried out using a Gaussian distribution. The O 1s core level spectra show three deconvoluted binding energy peaks between 529−532 eV for both the bilayer ZnO CBLs.[38−40] The lower binding energy (529.48 eV) peak that is attributed to O atoms in the wurtzite ZnO structure of the hexagonal Zn^{2+} ions for bilayer ZnO NRs/ZnO SG shifts toward lower energy by 0.13 eV in comparison to that in ZnO SG/ZnO NRs.[39] Moreover, the intensity of lower binding energy O 1s peak is lower for ZnO NRs/ZnO SG compared to ZnO SG/ZnO NRs CBL. The second peak centered at 531.08 eV for ZnO NRs/ZnO SG corresponds to the loosely bounded oxygen ions on the surface, namely, OH^- groups or O^{2-} ions in oxygen vacancies in the ZnO matrix shifts toward the lower binding energy and has higher intensity than that in ZnO SG/ZnO NRs.[40,41] The above result shows that bilayer ZnO NRs/ZnO SG is more oxygen deficient or Zn rich which helps to form a stable ZnO film. Additionally, it is well-known that oxygen deficient films

DOI: 10.1021/am509125c
ACS Appl. Mater. Interfaces 2015, 7, 7951−7960

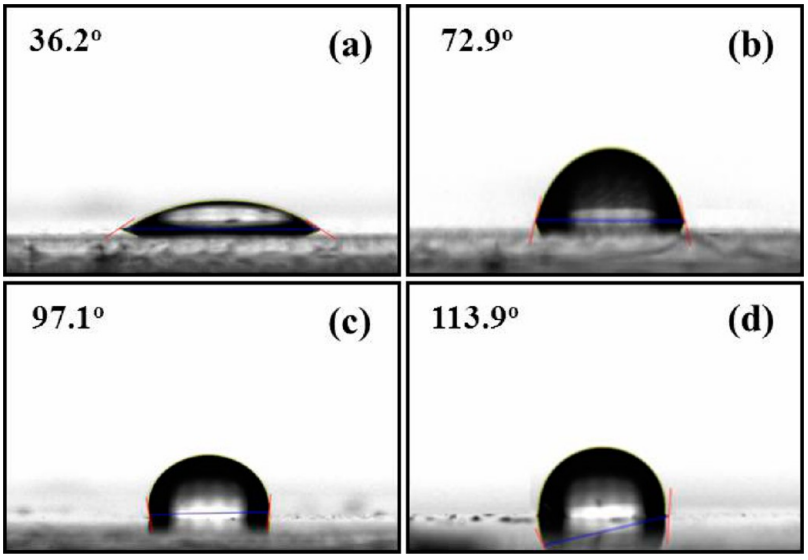

Figure 7. Contact angle measurements before and after P3HT:PCBM photoactive coating, respectively, on (a, c) ZnO SG/ZnO NRs and (b, d) ZnO NRs/ZnO SG CBLs surface, respectively.

possess high conductivity, which is further confirmed in the Hall analysis (explained below).

Another peak centered at 532.61, ascribed to chemisorbed ions (OH^- or O^{2-}) on the surface of ZnO in the oxygen deficient region is found to be shifted toward higher binding energy in ZnO NRs/ZnO SG.[38] This binding energy shift may be a consequence of changes in the Fermi level within the band gap, caused by the transfer of electrons within the bilayer ZnO or band bending.[42] This result indicates that the structure and stoichiometry of bilayer ZnO NRs/ZnO SG is better than that of ZnO SG/ZnO NRs.

Current density−voltage ($J-V$) measurements of IOSCs incorporating bilayer ZnO CBL with optimized annealing temperatures are shown in Figure 6. Table 1 summarizes the device parameters of bilayer CBL IOSCs. The photovoltaic performance is found to be dependent on the morphology and annealing temperature of ZnO nanostructures. The IOSC device comprising bilayer CBL of ZnO NRs/ZnO SG exhibited PCE as high as 3.70% that is ∼14% higher compared to the reference devices of single layer CBLs (data presented in SI Table S1). The enhancement in PCE is majorly influenced by the increased J_{sc} in the IOSCs of bilayer ZnO compared to single layer CBLs, which indicates that the bilayer ZnO nanostructured CBLs promote more favorable electron transport within the device. This is attributed to the increased interfacial contact between the photoactive layer and denser ZnO NRs/ZnO SG CBL. For ZnO NRs/ZnO SG, an enhanced dissociation of photogenerated excitons takes place leading to larger number of electrons and holes. This generates more percolation pathways leading to the improved electron transport, and thus increased photocurrent density.

The comparison of $J-V$ measurements (Figure 6a) for IOSCs employing bilayer ZnO CBLs shows significant enhancement in photovoltaic parameters in ZnO NRs/ZnO SG device with respect to that of ZnO SG/ZnO NRs. Bilayer device with ZnO NRs/ZnO SG presents notable increment in J_{sc} from 9.48 to 10.66 (mA/cm^2) and V_{oc} from 0.58 to 0.61 V. The increased J_{sc} in ZnO NRS-ZnO SG is supported by enhancement in External quantum efficiency (EQE) (Figure 6b). It is found that the IOSCs of ZnO NRs/ZnO SG exhibited an EQE of 66.7% in contrast to a lower EQE of 58.4% for IOSCs comprising of ZnO SG/ZnO NRs CBLs, indicating much efficient photon to current conversion in the devices of ZnO NRs/ZnO SG. The increased EQE in IOSCs of ZnO NRs/ZnO SG is due to the enhanced light absorption (as evident from higher transmittance) and charge collection efficiency (explained further using EIS analysis). The integrated EQE values are all in good agreement with the enhanced J_{sc}.

In order to investigate the origin of enhanced J_{sc}, photoluminescence (PL) quenching study of bilayer ZnO CBLs was carried out (SI Figure S8). The PL quenching is a useful indication of the efficient charge transfer and exciton dissociation between donor−acceptor materials.[43] PL quenching was carried out on both the samples using P3HT-only and an organic blend of P3HT:PCBM, separately. To avoid the effect of light scattering through the glass substrate, PL measurements were carried out from the side of P3HT.[44] The comparison of PL intensities (SI Figure S8a) for both bilayer acceptors reveal higher quenching in the films of ZnO NRs/ZnO SG indicating higher charge transfer efficiency from P3HT to ZnO NRs/ZnO SG compared to that to ZnO SG/ZnO NRs. The enhanced PL quenching in ZnO NRs/ZnO SG is indicative of faster deactivation of the excited state by the efficient charge transfer between P3HT and bilayer ZnO NRs/ZnO SG and is attributed to improved heterojunction between the acceptor and the donor.

The sandwiching of more compact ZnO SG layer between ZnO NRs and P3HT offers a greater interfacial contact to extract electrons more effectively after excitonic dissociation. However, this is not the case when ZnO NRs are sandwiched between ZnO SG and P3HT (in the case of devices of ZnO SG/ZnO NRs) although sandwiched ZnO NRs also offer a better contact. This is attributed to the fact that ZnO SG is known to be a much efficient electron extractor as compared to ZnO NRs.[29] Moreover, a very strong PL quenching (SI Figure S8b) is observed in the films of P3HT:PCBM BHJ blend coated on ZnO NRs/ZnO SG owing to the preferential enrichment of P3HT phase on a comparatively hydrophobic ZnO NRs/ZnO SG (water contact angle 72.9°). It is thus logical to believe that the presence of ZnO SG over ZnO NRs

DOI: 10.1021/am509125c
ACS Appl. Mater. Interfaces 2015, 7, 7951−7960

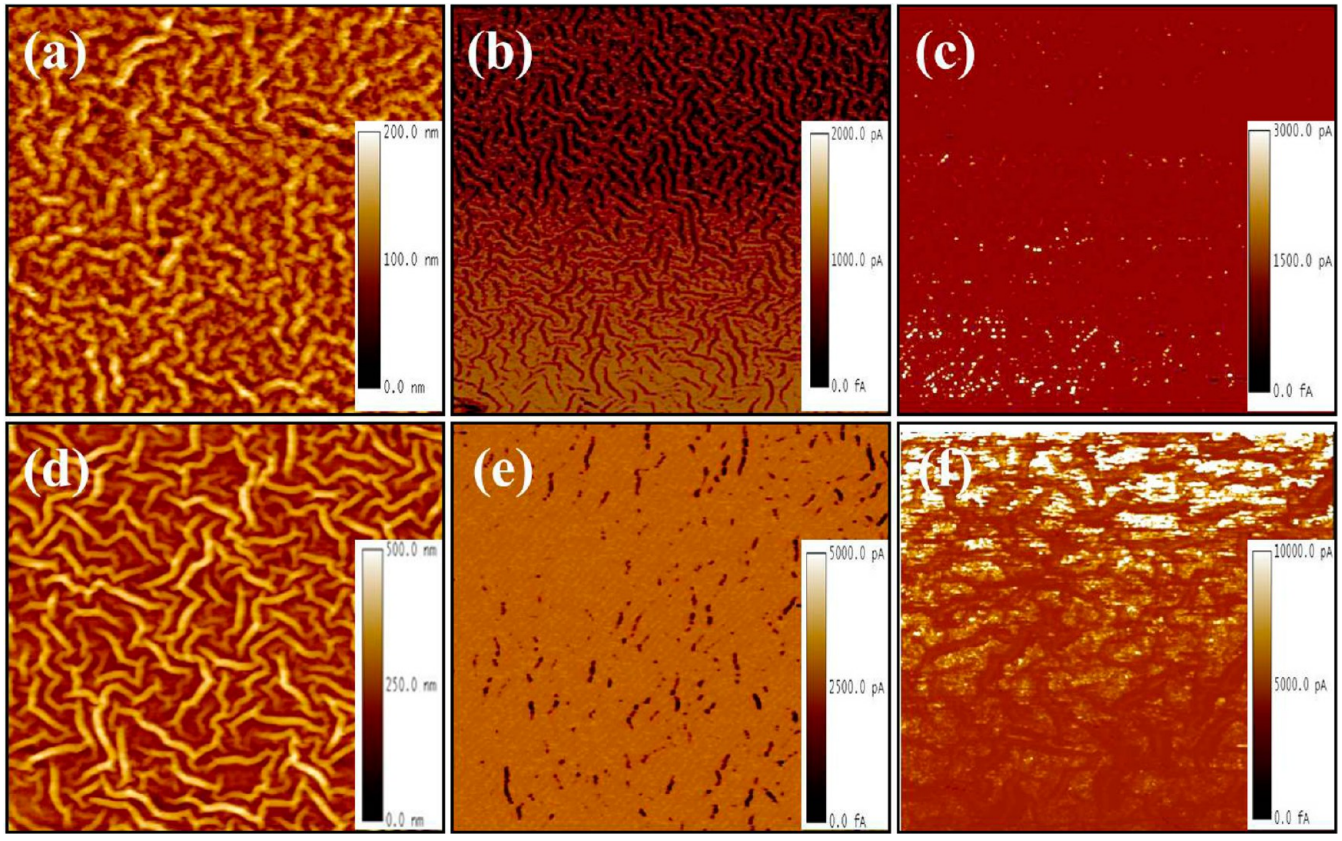

Figure 8. (a) AFM topography and (b) corresponding C-AFM maps at −10 V and (c) +10 V for bilayer ZnO SG/ZnO NRs CBL. (d) AFM topograph and (e) corresponding C-AFM maps at −10 and , (f) +10 V for bilayer ZnO NRs/ZnO SG CBL. Active region in reverse bias corresponds to hole conduction pathways, and active region in forward bias corresponds to electron conduction pathways.

(ZnO NRs/ZnO SG) is extremely beneficial in improving the electron extraction as compared to ZnO NRs over ZnO SG (ZnO SG/ZnO NRs). Furthermore, a lower value of R_s found in bilayer ZnO NRs/ZnO SG denotes decreased surface traps that may inhibit the trap assisted recombinations by enhancing the electron coupling with the photoactive layer followed by efficient charge transportation. The increased contact resistance and lower exciton dissociation efficiency of bilayer ZnO SG/ZnO NRs results in lower photovoltaic performance.

Additionally, the enhanced electrical properties of bilayer ZnO NRs/ZnO SG are supported by ∼22.6% higher electron mobility and ∼23.91% higher carrier density in comparison to ZnO SG/ZnO NRs, elucidated by Hall-effect measurements based on Van der Pauw method (SI Table S2) at room temperature.[45] The enhancement in electron mobility is due to the minimization of grain boundary scattering resulting from a denser morphology of ZnO NRs/ZnO SG. On the other hand, the decrease in charge carrier mobility in the case of ZnO SG/ZnO NRs is associated with serious morphological distortions, especially in the bottom layer (ZnO SG), which typically leads to trapping of charges and retardation of flow to the cathode (ITO). Furthermore, the electrical conductivity for bilayer ZnO NRs/ZnO SG was found to be 46.85% higher compared to ZnO SG/ZnO NRs. This phenomenon can be attributed to the improvement in crystallinity of ZnO NRs/ZnO SG.[46] The electrical properties are in good agreement with the FE-SEM, XRD, PL and device results for both the bilayer CBLs. It is thus evident that the electrical properties are strongly influenced by appropriate layering sequence of ZnO morphologies.

To cognize the mechanism of performance enhancement in the IOSCs of bilayer ZnO, CBLs were investigated by performing multiple advancing water contact angle from different positions, before and after coating of photoactive layers (shown in Figure 7). The lower contact angle (36°) exhibited by ZnO SG/ZnO NRs reveals hydrophilic nature and is attributed to its distorted morphology as well as formation of large ZnO aggregates in the interface between ITO and CBL. Lower hydrophilicity and formation of aggregates results in large interfacial contact resistance as well as bulk resistance leading to decreased photovoltaic performance in IOSCs of ZnO SG/ZnO NRs.[30,47] Meanwhile, the contact angle of ZnO NRs/ZnO SG (Figure 7b) with a uniform, compact and dense morphology is measured to be 72.9°. An increase in water contact angle shows significant transition in surface properties from hydrophilic to hydrophobic that is beneficial for the intimate contact between bilayer ZnO and the photoactive layer, which ultimately leads to a decrease in series resistance. Figure 7c and d shows the digital images of contact angles measured on photoactive layer spin-coated on bilayer CBLs. Higher contact angle of 113.9° for ZnO NRs/ZnO SG coated with photoactive layer is suggestive of better interfacial contact and effective electron transport than that in photoactive covered ZnO SG/ZnO NRs, which exhibited a lower contact angle of only 97.1°. Thus, it is obvious to obtain higher J_{sc} in the IOSCs of former than in later.

Electrical properties of bilayer ZnO were elucidated using conductive atomic force microscopy (C-AFM) measured in contact mode. C-AFM is recognized as one of the useful techniques for high resolution characterization of local electrical

DOI: 10.1021/am509125c
ACS Appl. Mater. Interfaces 2015, 7, 7951−7960

properties and morphologies.[48,49] Herein, forward and reverse biased electric fields were applied to both the bilayer CBLs. In the forward bias, electrons are injected while in the reverse bias, holes are injected through the conducting platinum-coated cantilever tip. By applying −10 and +10 V bias voltages between the AFM tip and the conducting bilayer ZnO CBL, current and hole maps were obtained as seen in Figure 8. Active regions in reverse bias corresponds to hole conduction pathways and those in forward bias correspond to electron conduction pathways.[50] Comparing Figure 8b,c and e,f, it is evident that, under the reverse bias condition, ZnO SG/ZnO NRs is hole dominant (darker regions), while in the forward bias ZnO NRs/ZnO SG is electron dominant (bright regions). This result shows that electric conduction is superior in ZnO NRs/ZnO SG compared to ZnO SG/ZnO NRs. Moreover, average current transported through ZnO NRs/ZnO SG is 10 000 pA, while that through ZnO SG/ZnO NRs is 3000 pA (Figure 8c−f). Thus, electrical conduction in bilayer ZnO NRs/ZnO SG is higher by a factor of ∼3.33 than that of bilayer ZnO SG/ZnO NRs, demonstrating an enhancement in charge transport in the previous case than in latter. The increased surface conductivity in bilayer ZnO NRs/ZnO SG leads to generation of more channels for electron transport. Thus, the emergence of higher J_{sc} in IOSCs of ZnO NRs/ZnO SG is justified.

In order to verify energy level arrangement and evaluate the enhancement of V_{oc} using bilayer ZnO CBL, ultraviolet photoelectron spectroscopy (UPS) measurements were carried out. The high binding energy cut off (E_{cutoff}) for both the bilayer is shown in Figure 9a. The valence band maximum (VBM) energy levels are calculated using eq 1.[51]

$$\mathrm{VBM} = h\nu - (E_{\mathrm{cutoff}} - E_{\mathrm{onset}}) \quad (1)$$

where $h\nu$ = 21.22 eV is the incident photon energy and E_{onset} is the onset relative to the Fermi level (EF) of Au (at 0 eV). EF is determined from the Au substrate. From Table 2, the calculated

Table 2. Energy Levels of Bilayer ZnO CBLs Derived from UPS Measurements

bilayer ZnO CBL	E_{cutoff} (eV)	E_{onset} (eV)	VBM (eV)	CBM (eV)
ZnO SG 170 °C/ ZnO NRs 270 °C	16.95	3.26	−7.53	−4.23
ZnO NRs 270 °C/ ZnO SG 170 °C	16.98	3.42	−7.66	−4.38

E_{cutoff} values of bilayer ZnO SG/ZnO NRs and ZnO NRs/ZnO SG were 16.95 and 16.98 eV, respectively. The E_{onset} is the highest occupied molecular orbital (HOMO) energy onset, referred to as the binding-energy onset. The onsets for bilayer ZnO SG/ZnO NRs and ZnO NRs/ZnO SG are 3.26 and 3.42 eV, respectively. From the VBM energies and optical gaps obtained from the onset of absorption spectra, the estimated conduction band minimum (CBM) positions with respect to vacuum are −4.23 and −4.38 eV, respectively.[22] The corresponding VBM energy levels are −7.53 and −7.66 eV (Table 2). The corresponding energy band diagram is illustrated in Figure 9c.

The optical band gap energies (E_g) of bilayer CBLs were estimated using the formula.

$$(\alpha h\nu)^2 = A(h\nu - E_g) \quad (2)$$

where A is the proportional constant, α is the absorption coefficient, h is Planck's constant, ν is frequency of vibration light, and E_g is the band gap.[52] SI Figure S10a shows $(\alpha h\nu)^2$ plotted as a function of photon energy for bilayer CBLs. The direct optical band gap energies of bilayer CBLs were determined by extrapolating the linear portion of the curves near the onset of the absorption edge to the energy axis. The optical band gap energies are 3.30 and 3.28 eV for bilayer ZnO SG/ZnO NRs and ZnO NRs/ZnO SG, respectively. The reduced band gap energy of ZnO NRs/ZnO SG CBL can lead to a large built-in potential and ultimately will enhance the charge collection efficiency. Further reduced E_g of bilayer ZnO NRs/ZnO SG CBL is suggestive of decreased surface traps, which would restrain the possible trap assisted interfacial charge recombination. This confirms that the ZnO NRs/ZnO SG could reduce the E_g and consequently enhance the light-absorption properties, and thus improve the PCE of IOSCs.[53]

Furthermore, the work function of bilayer CBLs was evaluated using AC2 photoelectron spectrometer; the UV source was employed to measure the ionization potential in air. SI Figure S10b plots the square root of the counting rate as a function of photon energy and the photoemission threshold energy also known as work function were measured from crossing point of the background and the yield line.[54] The work functions of bilayer ZnO SG/ZnO NRs and ZnO NRs-SG CBLs, presented in SI Table S3, are 4.23 and 4.35 eV, respectively. These results suggest that the sequencing of nanostructures in bilayer configuration is influential in tuning the energy level alignment of the device.

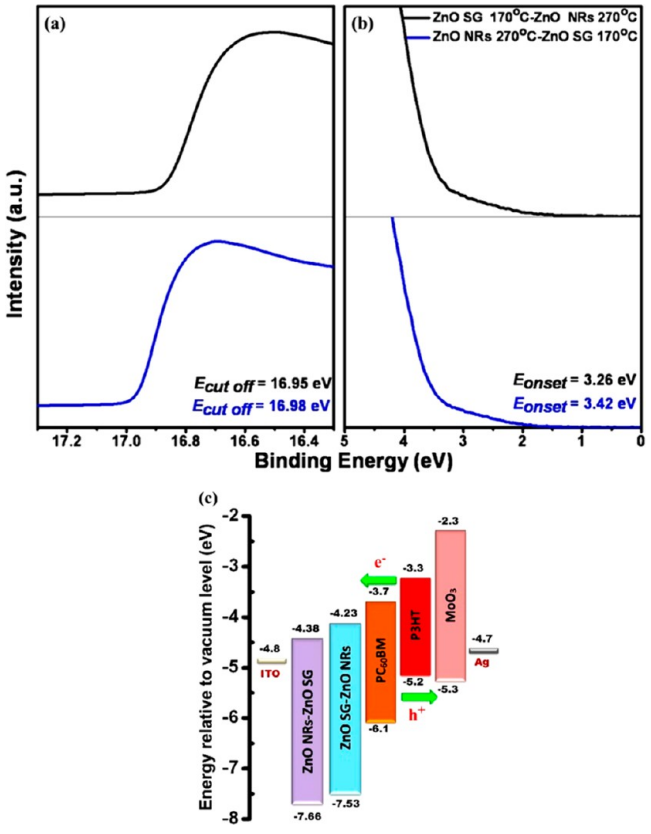

Figure 9. UPS spectra of bilayer ZnO CBLs: (a) cutoff region, (b) onset region, and (c) corresponding energy level diagram.

DOI: 10.1021/am509125c
ACS Appl. Mater. Interfaces 2015, 7, 7951−7960

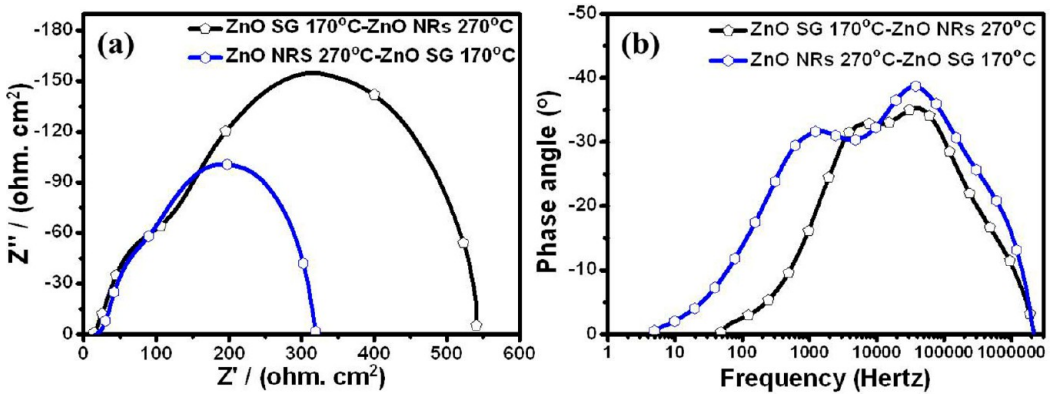

Figure 10. (a) Nyquist and (b) Bode phase plots of bilayer ZnO CBLs.

The enhancement in the device performance is majorly from the improvement of the heterojunction interface between the bilayer ZnO CBL and photoactive layer. Furthermore, to evaluate the genesis of improved electrical characteristics in bilayer ZnO CBLs, electrochemical impedance spectroscopy (EIS, Figure 10) and Mott−Schottky (MS, SI Figure S11b) measurements were performed to investigate charge transfer and flat band potential (V_{fb}), respectively. EIS is an effective technique to study the interface and bulk electronic properties of OSCs.[55] Figure 10a presents Nyquist plots of the devices measured under simulated 1 sun illumination at zero bias. The EIS plots were fitted using an equivalent circuit as illustrated in SI Figure S11a.[56] The Nyquist plots show distinct semicircles in high and low frequency range corresponding to different charge transfer mechanisms in IOSCs of both the bilayer ZnO CBLs. The semicircle in high frequency range corresponds to the recombination of charges ascribed to electron transfer at the interface between bilayer ZnO CBL and P3HT: PCBM BHJ.[57] As seen in Figure 10a, both the semicircles for bilayer ZnO NRs/ZnO SG show significant reduction in the charge transfer resistance at the interface between CBL and active layer as compared to ZnO SG/ZnO NRs. This is attributed to the enhancement of ohmic contact between the hydrophobic bilayer ZnO NRs/ZnO SG CBLs with the organic photoactive BHJ layer.

Electron lifetime (τ) in IOSCs was measured from the Bode phase plots (Figure 10b). Bode phase angle vs frequency plots were plotted, and τ was calculated according to eq 3.

$$\tau = (1/2\pi f_{max}) \quad (3)$$

where f_{max} is the maximum frequency of the mid frequency peak.[58] The τ values estimated from Bode's phase plots are 2.24×10^{-5} and 1.29×10^{-4} ms for bilayers ZnO SG/ZnO NRs and ZnO NRs/ZnO SG, respectively. For ZnO NRs/ZnO SG CBL, the increased electron lifetime is due to reduced charge transfer resistance and decreased electron recombination which makes electron transfer more efficient leading to the enhancement of device performance. Thus, it is to be noted that photogenerated charge carrier transport is facilitated through the incorporation of bilayer ZnO NRs/ZnO SG between ITO and photoactive layer. It is inferred that, in the presence of bilayer ZnO NRs/ZnO SG, (a) electrons are effectively collected/extracted by ZnO SG from the photoactive layer, and (b) they are further transported effectively through ZnO NRs to the cathode (ITO) leading to the enhancement of efficiency. Thus, this bilayer buffer layer plays dual role in the IOSCs: one of electron extraction (ZnO SG)[29] and second of electron transportation (ZnO NRs).[25] The above results indicate that the superior electrical properties of bilayer ZnO NRs/ZnO SG CBL are advantageous in facilitating the increased charge transfer efficiency and photovoltaic performance.

CONCLUSIONS

In summary, we have successfully demonstrated bilayer ZnO as CBLs in efficient IOSCs. This strategy to integrate bilayer ZnO plays a dual role: electron extraction/collection from the photoactive layer and its transportation to the cathode (ITO). The hydrophobic nature of bilayer ZnO NRs/ZnO SG CBLs with the photoactive layer has improved the interfacial contact for efficient charge transfer. With introduction of bilayer ZnO NRs/ZnO SG CBLs, defect levels are minimized while retaining the native structure morphology. C-AFM investigations and other physical and optical measurements reveal that the highly transparent bilayer ZnO NRs/ZnO SG CBL not only forms the uniform film between the cathode and photoactive layer but also improves the electrical properties in addition to photovoltaic performance. When the sequence of bilayer ZnO CBLs is reversed, the photovoltaic performance of the device is drastically reduced because of the morphology destruction and poor electrical properties. The annealing, morphology and geometry of bilayer ZnO should be precisely controlled for enhancing the device performance. The optimization of bilayer ZnO NRs/ZnO SG CBL demonstrated an enhanced J_{sc} from 9.48 to 10.66 mA cm^2 and V_{oc} from 0.58 to 0.61 V. As high as 3.70% PCE is achieved for the optimized bilayer ZnO NRs/ZnO SG CBL in IOSCs. We believe our findings will provide a new insight of selecting appropriate bilayer CBL in the IOSCs that can play dual electron extraction and electron transport functions.

ASSOCIATED CONTENT

Supporting Information

Experimental details, structural characterizations, and supplementary figures and tables. This material is available free of charge via the Internet at http://pubs.acs.org.

AUTHOR INFORMATION

Corresponding Author

*E-mail: shlee66@jbnu.ac.kr. Tel: +82 63 270 2435. Fax: +82 63 270 2306.

Notes

The authors declare no competing financial interest.

DOI: 10.1021/am509125c
ACS Appl. Mater. Interfaces 2015, 7, 7951−7960

■ ACKNOWLEDGMENTS

This research was supported by the Pioneer Research Centre Program through the National Research Foundation of Korea funded by the Ministry of Science, ICT & Future Planning (NRF-2013M3C1A3065528).

■ REFERENCES

(1) Yu, G.; Gao, J.; Hummelen, J. C.; Wudl, F.; Heeger, A. J. Polymer Photovoltaic Cells: Enhanced Efficiencies via a Network of Internal Donor-Acceptor Heterojunctions. *Science* **1995**, *270*, 1789−1791.

(2) Ma, W. L.; Yang, C. Y.; Gong, X.; Lee, K.; Heeger, A. J. Thermally Stable, Efficient Polymer Solar Cells with Nanoscale Control of the Interpenetrating Network Morphology. *Adv. Funct. Mater.* **2005**, *15*, 1617−1622.

(3) Janssen, R. A. J.; Nelson, J. Factors Limiting Device Efficiency in Organic Photovoltaics. *Adv. Mater.* **2013**, *25*, 1847−1858.

(4) Jun, G. H.; Jin, S. H.; Lee, B.; Kim, B. H.; Chae, W. S.; Hong, S. H.; Jeon, S. Enhanced Conduction and Charge-Selectivity by N doped Graphene Flakes in the Active Layer of Bulk Heterojunction Organic Solar Cells. *Energy Environ. Sci.* **2013**, *6*, 3000−3006.

(5) Yip, H. L.; Jen, A. K. Y. Recent Advances in Solution-processed Interfacial Materials for Efficient and Stable Polymer Solar Cells. *Energy Environ. Sci.* **2012**, *5*, 5994−6011.

(6) Ameri, T.; Dennler, G.; Lungenschmied, C.; Brabec, C. J. Organic Tandem Solar Cells: A Review. *Energy Environ. Sci.* **2009**, *2*, 347−363.

(7) Li, G.; Shrotriya, V.; Huang, J.; Yao, Y.; Moriarty, T.; Emery, K.; Yang, Y. High-efficiency Solution Processable Polymer Photovoltaic Cells by Self-Organization of Polymer Blends. *Nat. Mater.* **2005**, *4*, 864−868.

(8) Padinger, F.; Rittberger, R. S.; Sariciftci, N. S. Effects of Postproduction Treatment on Plastic Solar Cells. *Adv. Funct. Mater.* **2003**, *13*, 85−88.

(9) Zilberberg, K.; Trost, S.; Meyer, J.; Kahn, A.; Behrendt, A.; Lützenkirchen-Hecht, D.; Frahm, R.; Riedl, T. Inverted Organic Solar Cells with Sol−Gel Processed High Work-Function Vanadium Oxide Hole-Extraction Layers. *Adv. Funct. Mater.* **2011**, *21*, 4776−4783.

(10) Dang, M. T.; Hirsch, L.; Wantz, G. P3HT:PCBM, Best Seller in Polymer Photovoltaic Research. *Adv. Mater.* **2011**, *23*, 3597−3602.

(11) Jørgensen, M.; Norrman, K.; Krebs, F. C. Stability/Degradation of Polymer Solar Cells. *Sol. Energy Mater. Sol. Cells* **2008**, *92*, 686−714.

(12) Xu, Z.; Chen, L.-M.; Yang, G.; Huang, C.-H.; Hou, J.; Wu, Y.; Li, G.; Hsu, C.-S.; Yang, Y. Vertical Phase Separation in Poly(3-hexylthiophene): Fullerene Derivative Blends and its Advantage for Inverted Structure Solar Cells. *Adv. Funct. Mater.* **2009**, *19*, 1227−1234.

(13) Zou, J.; Yip, H. L.; Zhang, Y.; Gao, Y.; Chien, S. C.; O'Malley, K.; Chueh, C. C.; Chen, H.; Jen, A. K. Y. High-Performance Inverted Polymer Solar Cells: Device Characterization, Optical Modeling, and Hole-Transporting Modifications. *Adv. Funct. Mater.* **2012**, *22*, 2804−2811.

(14) Lee, Y. J.; Yi, J.; Gao, G. F.; Koerner, H.; Park, K.; Wang, J.; Luo, K.; Vaia, R. A.; Hsu, J. W. P. Low-Temperature Solution-Processed Molybdenum Oxide Nanoparticle Hole Transport Layers for Organic Photovoltaic Devices. *Adv. Energy Mater.* **2012**, *2*, 1193−1197.

(15) Subbiah, J.; Amb, C. M.; Irfan, I.; Gao, Y.; Reynolds, J. R.; So, F. High-Efficiency Inverted Polymer Solar Cells with Double Interlayer. *ACS Appl. Mater. Interfaces* **2012**, *4*, 866−870.

(16) Huang, J.; Yinb, Z.; Zheng, Q. Applications of ZnO in Organic and Hybrid Solar Cells. *Energy Environ. Sci.* **2011**, *4*, 3861−3877.

(17) Zilberberg, K.; Meyerb, J.; Riedl, T. Solution Processed Metal-Oxides for Organic Electronic Devices. *J. Mater. Chem. C* **2013**, *1*, 4796−4815.

(18) Tan, M. J.; Zhong, S.; Li, J.; Chen, Z.; Chen, W. Air-Stable Efficient Inverted Polymer Solar Cells Using Solution-Processed Nanocrystalline ZnO Interfacial Layer. *ACS Appl. Mater. Interfaces* **2013**, *5*, 4696−4701.

(19) Shao, S.; Zheng, K.; Pullerits, T.; Zhang, F. Enhanced Performance of Inverted Polymer Solar Cells by Using Poly (ethylene oxide)-Modified ZnO as an Electron Transport Layer. *ACS Appl. Mater. Interfaces* **2013**, *5*, 380−385.

(20) Steim, R.; Koglera, F. R.; Brabec, C. J. Interface Materials for Organic Solar Cells. *J. Mater. Chem.* **2010**, *20*, 2499−2512.

(21) Liang, Z.; Zhang, Q.; Wiranwetchayan, O.; Xi, J.; Yang, Z.; Park, K.; Li, C.; Cao, G. Effects of the Morphology of a ZnO Buffer Layer on the Photovoltaic Performance of Inverted Polymer Solar Cells. *Adv. Funct. Mater.* **2012**, *22*, 2194−2201.

(22) Sun, Y.; Seo, J. H.; Takacs, C. J.; Seifter, J.; Heeger, A. J. Inverted Polymer Solar Cells Integrated with a Low-Temperature-Annealed Sol-Gel-Derived ZnO Film as an Electron Transport Layer. *Adv. Mater.* **2011**, *23*, 1679−1683.

(23) Huang, J. H.; Wei, H. Y.; Huang, K. C.; Chen, C. L.; Wang, R. R.; Chen, F. C.; Ho, K. C.; Chu, C. W. Using a Low Temperature Crystallization Process to Prepare Anatase TiO_2 Buffer Layers for Air-stable Inverted Polymer Solar Cells. *Energy Environ. Sci.* **2010**, *3*, 654−658.

(24) Yang, H. B.; Dong, Y. Q.; Wang, X.; Khoo, S. Y.; Liu, B. Cesium Carbonate Functionalized Graphene Quantum Dots as Stable Electron-Selective Layer for Improvement of Inverted Polymer Solar Cells. *ACS Appl. Mater. Interfaces* **2014**, *6*, 1092−1099.

(25) Ambade, S. B.; Ambade, R. B.; Lee, W.; Mane, R. S.; Yoon, S. C.; Lee, S. H. Development of Highly Transparent Seedless ZnO Nanorods Engineered for Inverted Polymer Solar Cells. *Nanoscale* **2014**, *6*, 12130−12141.

(26) Kim, S.; Kim, C. H.; Lee, S. K.; Jeong, J. H.; Lee, J.; Jin, S. H.; Shin, W. S.; Song, C. E.; Choi, J. H.; Jeong, J. R. Highly Efficient Uniform ZnO Nanostructures for an Electron Transport Layer of Inverted Organic Solar Cells. *Chem. Commun.* **2013**, *49*, 6033−6035.

(27) Cheun, H.; Hernandez, C. F.; Zhou, Y.; Potscavage, W. J., Jr; Kim, S. J.; Shim, J.; Dindar, A.; Kippelen, B. Electrical and Optical Properties of ZnO Processed by Atomic Layer Deposition in Inverted Polymer Solar Cells. *J. Phys. Chem. C* **2010**, *114*, 20713−20718.

(28) Sanchez, S.; Berson, S.; Guillerez, S.; Lévy-Clément, C.; Ivanova, V. Toward High-Stability Inverted Polymer Solar Cells with an Electrodeposited ZnO Electron Transporting Layer. *Adv. Energy Mater.* **2012**, *2*, 541−545.

(29) Sekine, N.; Chou, C. H.; Kwan, W. L.; Yang, Y. ZnO Nano-ridge Structure and its Application in Inverted Polymer Solar Cell. *Org. Electron.* **2009**, *10*, 1473−1477.

(30) Ma, Z.; Tang, Z.; Wang, E.; Andersson, M. R.; Inganäs, O.; Zhang, F. Influences of Surface Roughness of ZnO Electron Transport Layer on the Photovoltaic Performance of Organic Inverted Solar Cells. *J. Phys. Chem. C* **2012**, *116*, 24462−24468.

(31) Takanezawa, K.; Hirota, K.; Wei, Q. S.; Tajima, K.; Hashimoto, K. Efficient Charge Collection with ZnO Nanorod Array in Hybrid Photovoltaic Devices. *J. Phys. Chem. C* **2007**, *111*, 7218−7223.

(32) Guo, L.; Ji, Y. L.; Xu, H. Regularly Shaped, Single-Crystalline ZnO Nanorods with Wurtzite Structure. *J. Am. Chem. Soc.* **2002**, *124*, 14864−14865.

(33) Zhang, R.; Kumar, S.; Zou, S.; Kerr, L. L. High-Density Vertically Aligned ZnO Rods with a Multistage Terrace Structure and Their Improved Solar Cell Efficiency. *Cryst. Growth Des.* **2008**, *8*, 381−383.

(34) Lee, Y. C.; Hub, S. Y.; Water, W.; Tiong, K. K.; Feng, Z. C.; Chen, Y. T.; Huang, J. C.; Lee, J. W.; Huang, C. C.; Shen, J. L.; Cheng, M. H. Rapid Thermal Annealing Effects on the Structural and Optical Properties of ZnO Films Deposited on Si Substrates. *J. Lumin.* **2009**, *129*, 148−152.

(35) Zhou, H. M.; Yi, D. Q.; Yu, Z. M.; Xiao, L. R.; Li, J. Preparation of Aluminum Doped Zinc Oxide Films and the Study of their Microstructure, Electrical and Optical Properties. *Thin Solid Films* **2007**, *515*, 6909−6914.

(36) Lee, J. H.; Ko, K. H.; Park, B. O. Electrical and Optical Properties of ZnO Transparent Conducting Films by the Sol−gel Method. *J. Cryst. Growth* **2003**, *247*, 119−125.

(37) *Handbook of X-ray Photoelectron Spectroscopy*; Muilenbenger, G. E., Ed.; Perkin-Elmer Corporation: Eden Prarie, MN, 1979.

DOI: 10.1021/am509125c
ACS Appl. Mater. Interfaces 2015, 7, 7951−7960

(38) Islam, M. N.; Ghosh, T. B.; Chopra, K. L.; Acharya, H. N. XPS and X-ray Diffraction Studies of Aluminum-doped Zinc Oxide Transparent Conducting Films. *Thin Solid Films* **1996**, *280*, 20−25.
(39) Wang, Z.; Hou, J.; Yang, C.; Jiao, S.; Huang, K.; Zhu, H. Template-free Synthesis of 3D Nb_3O_7F Hierarchical Nanostructures and Enhanced Photocatalytic Activities. *Phys. Chem. Chem. Phys.* **2013**, *15*, 3249−3255.
(40) Lu, W.; Gao, S.; Wang, J. One-Pot Synthesis of Ag/ZnO Self-Assembled 3D Hollow Microspheres with Enhanced Photocatalytic Performance. *J. Phys. Chem. C* **2008**, *112*, 16792−16800.
(41) Ramgir, N. S.; Mulla, I. S.; Pillai, V. K. Micropencils and Microhexagonal Cones of ZnO. *J. Phys. Chem. B* **2006**, *110*, 3995−4001.
(42) Tam, K. H.; Cheung, C. K.; Leung, Y. H.; Djurišić, A. B.; Ling, C. C.; Beling, C. D.; Fung, S.; Kwok, W. M.; Chan, W. K.; Phillips, D. L.; Ding, L.; Ge, W. K. Defects in ZnO Nanorods Prepared by a Hydrothermal Method. *J. Phys. Chem. B* **2006**, *110*, 20865−20871.
(43) Ruankham, P.; Sagawa, T.; Sakaguchi, H.; Yoshikawa, S. Vertically Aligned ZnO Nanorods Doped with Lithium for Polymer Solar Cells: Defect Related Photovoltaic Properties. *J. Mater. Chem.* **2011**, *21*, 9710−9715.
(44) Gadisa, A.; Liu, Y.; Samulski, E. T.; Lopez, R. Role of Thin *n*-Type Metal-Oxide Interlayers in Inverted Organic Solar Cells. *ACS Appl. Mater. Interfaces* **2012**, *4*, 3846−3851.
(45) Cheun, H.; Hernandez, C. F.; Shim, J.; Fang, Y.; Cai, Y.; Li, H.; Sigdel, A. K.; Meyer, J.; Maibach, J.; Dindar, A.; Zhou, Y.; Berry, J. J.; Bredas, J. L.; Kahn, A.; Sandhage, K. H.; Kippelen, B. Oriented Growth of Al_2O_3:ZnO Nanolaminates for Use as Electron-Selective Electrodes in Inverted Polymer Solar Cells. *Adv. Funct. Mater.* **2012**, *22*, 1531−1538.
(46) Kima, H.; Piqúeb, A.; Horwitzb, J. S.; Muratab, H.; Kafafib, Z. H.; Gilmorea, C. M.; Chrisey, D. B. Effect of Aluminum Doping on Zinc Oxide Thin Films Grown by Pulsed Laser Deposition for Organic Light-Emitting Devices. *Thin Solid Films* **2000**, *377*, 798−802.
(47) Shinde, V. R.; Lokhande, C. D.; Mane, R. S.; Han, S. H. Hydrophobic and Textured ZnO Films Deposited by Chemical Bath Deposition: Annealing Effect. *Appl. Surf. Sci.* **2005**, *245*, 407−413.
(48) He, Z.; Phan, H.; Liu, J.; Nguyen, T. Q.; Tan, T. T. Y. Understanding TiO_2 Size-Dependent Electron Transport Properties of a Graphene-TiO_2 Photoanode in Dye-Sensitized Solar Cells Using Conducting Atomic Force Microscopy. *Adv. Mater.* **2013**, *25*, 6900−6904.
(49) Zhou, H.; Zhang, Y.; Mai, C. K.; Collins, S. D.; Nguyen, T. Q.; Bazan, G. C.; Heeger, A. J. Conductive Conjugated Polyelectrolyte as Hole-Transporting Layer for Organic Bulk Heterojunction Solar Cells. *Adv. Mater.* **2014**, *26*, 780−785.
(50) Bull, T. A.; Pingree, L. S. C.; Jenekhe, S. A.; Ginger, D. S.; Luscombe, C. K. The Role of Mesoscopic PCBM Crystallites in Solvent Vapor Annealed Copolymer Solar Cells. *ACS Nano* **2009**, *3*, 627−636.
(51) Hu, T.; Li, F.; Yuan, K.; Chen, Y. Efficiency and Air-Stability Improvement of Flexible Inverted Polymer Solar Cells Using ZnO/Poly(ethylene glycol) Hybrids as Cathode Buffer Layers. *ACS Appl. Mater. Interfaces* **2013**, *5*, 5763−5770.
(52) Mane, R. S.; Lee, W. J.; Pathan, H. M.; Han, S. H. Nanocrystalline TiO_2/ZnO Thin Films: Fabrication and Application to Dye-Sensitized Solar Cells. *J. Phys. Chem. B* **2005**, *109*, 24254−24259.
(53) Stubhan, T.; Oh, H.; Pinna, L.; Krantz, J.; Litzov, I.; Brabec, C. J. Inverted Organic Solar Cells Using a Solution Processed Aluminum-doped Zinc Oxide Buffer Layer. *Org. Electron.* **2011**, *12*, 1539−1543.
(54) Chang, Y. M.; Wang, L.; Su, W. F. Polymer Solar Cells with Poly (3, 4-ethylenedioxythiophene) as Transparent Anode. *Org. Electron.* **2008**, *9*, 968−973.
(55) Huang, J.; Xu, Z.; Yang, Y. Low-Work-Function Surface Formed by Solution-Processed and Thermally Deposited Nanoscale Layers of Cesium Carbonate. *Adv. Funct. Mater.* **2007**, *17*, 1966−1973.
(56) Ambade, S. B.; Ambade, R. B.; Mane, R. S.; Lee, G. W.; Shaikh, S. F.; Patil, S. A.; Joo, O. S.; Han, S. H.; Lee, S. H. Low Temperature Chemically Synthesized Rutile TiO_2 Photoanodes with High Electron Lifetime for Organic Dye-Sensitized Solar Cells. *Chem. Commun.* **2013**, *49*, 2921−2923.
(57) Kuwabara, T.; Iwata, C.; Yamaguchi, T.; Takahashi, K. Mechanistic Insights into UV-Induced Electron Transfer from PCBM to Titanium Oxide in Inverted-Type Organic Thin Film Solar Cells Using AC Impedance Spectroscopy. *ACS Appl. Mater. Interfaces* **2010**, *2*, 2254−2260.
(58) Yuan, S.; Zhang, Y.; Liu, W.; Zhang, W. Efficient Inverted Organic Solar Cells using Zn-Doped Titanium Oxide Films as Electron Transport Layers. *Electrochim. Acta* **2014**, *116*, 442−446.

DOI: 10.1021/am509125c
ACS Appl. Mater. Interfaces 2015, 7, 7951−7960